

## Measurements and calculations of high-angular-momentum satellite transitions in Li 1s photoionization

W. T. Cheng,<sup>1,2</sup> E. Kukk,<sup>1,3</sup> D. Cubaynes,<sup>4</sup> J.-C. Chang,<sup>5</sup> G. Snell,<sup>1,3</sup> J. D. Bozek,<sup>3</sup> F. J. Wuilleumier,<sup>4</sup> and N. Berrah<sup>1</sup>

<sup>1</sup>*Department of Physics, Western Michigan University, Kalamazoo, Michigan 49008-5151*

<sup>2</sup>*Department of Physics, National Central University, Chung-Li, Taoyuan, Taiwan 32054, Republic of China*

<sup>3</sup>*Lawrence Berkeley National Laboratory, University of California, Berkeley, California, 94720*

<sup>4</sup>*Laboratoire de Spectroscopie Atomique et Ionique, CNRS UMR No. 8624, Université Paris-Sud, Bâtiment 350, 91405-Orsay, France*

<sup>5</sup>*Department of Mathematics and Science Education, National Hsinchu Teachers College, Hsinchu, Taiwan 300, Republic of China*

(Received 8 May 2000; published 13 November 2000)

Lithium 1s photoelectron spectra are reported in high electron and photon energy resolution, with resolved LS term structure of the  $\text{Li}^+$  1snl satellite transitions up to  $n=6$ . Branching ratios and anisotropy parameters of individual lines, determined over the 85–130 eV photon energy range, are compared with *R*-matrix calculations and with previous works. The high-angular-momentum satellite lines ( $L \geq 2$ ) are found to contribute significantly to the 1snl satellite cross sections for  $n=3$  and 4, and to become the dominant terms for  $n \geq 5$ . The high-angular-momentum lines exhibit the same photon-energy-dependence as the *P*-lines, providing experimental evidence that the continuum-continuum state coupling (equivalent to virtual electron collision processes) is responsible for the  $L \geq 1$  terms in the satellite spectrum, in contrast to the electron relaxation (shake-up) mechanism responsible for the *S*-terms. The angular distribution of the lines in the  $\text{Li}^+$  1snl,  $n=2-6$  groups, determined at 110 eV photon energy, is in good agreement with calculations, showing more isotropic distributions for high-angular-momentum lines.

PACS number(s): 32.30.-r

### I. INTRODUCTION

Two-electron atomic systems have been for many years the prototypical examples to study the electron correlations governing a three-particle system in a Coulomb field and the dynamics of its interaction with the electromagnetic field [1–4]. In order to advance further our understanding of more complex systems, one needs to understand the simplest example of a multielectron open-shell atom—the lithium atom. Its relatively simple structure allows highly-correlated calculations and the occupation of two electronic subshells opens the way to detailed investigation on inner-shell photoionization. During the past five years the study of the electronic structure and dynamics of lithium has stimulated great experimental and theoretical interest. Comparison of experimental data with *ab initio* calculations on the ground, excited, and ionic states of Li sheds light onto fundamental questions of electron correlation phenomena and advanced theoretical models. Photoelectron spectroscopy is particularly well suited for studying the electron correlation effects in Li, since correlation satellites observed in a photoelectron spectrum are a direct manifestation of electron correlations in atomic photoionization.

While numerous studies are available on the valence photoionization of Li, the 1s inner-shell photoemission has been less thoroughly investigated. The inner-shell regime became accessible in the late seventies with the development and use of synchrotron radiation sources. Such measurements proved to be difficult, however, due to the relatively small cross-section of the Li 1s photoionization in combination with low target atom densities of the evaporated atomic Li. In the early measurements [5], only the most general features of the spectra could be discerned due to the very low

experimental energy resolution and poor counting rates. It became apparent that the Li 1s photoelectron spectrum contains a rich satellite structure from the transitions to the 1snl ( $^{1,3}L$ ) final ionic states, which could provide valuable insights into electron correlation effects. Steady improvement of experimental conditions allowed measurements with more and more resolved 1s2l structures [6–10] as well as the angular distributions of the individual lines [7,8]. A comparison [7–9] of these measurements with available theoretical calculations [11–13] showed significant discrepancies, demonstrating that the understanding of the electron correlation processes even in such a simple system was far from being complete. More recently, the use of a modern third-generation synchrotron source has allowed to fully resolve the 1s2l photolines and partly the 1s3l lines in photoionization of lithium atoms in the  $1s^2 2s^2 S$  ground state [14,15] as well as in the  $1s^2 2p^2 P$  excited state [16,17]. Closely related to these works on correlation satellites, are also recent studies on multiple ionization of lithium atoms which involves two-electron and three-electron processes [18,19]. Simultaneously, highly-correlated calculations have also been performed to determine the partial cross sections for two-electron photoionization processes, including photoionization with excitation [20,21] and multiple ionization [22–24], highlighting the need for very high resolution measurements of high *n* photoelectron satellites to provide a more stringent test of theory. Clearly, effects such as configuration interaction and interchannel coupling become increasingly more important with increasing values of the principal quantum number. So far, no experimental results with fully-resolved LS term structure of the  $n > 2$  satellite lines have been reported. In the present study, we report on experimental and theoretical results on Li 1s photoionization. Li 1s

photoelectron spectra, with a total linewidth down to 37 meV, have been measured allowing the resolution of the  $1snl$  term structure completely for  $n=2$  and 3, and partially for  $n=4, 5$ , and 6, to the best of our knowledge, for the first time. Experimental branching ratios and angular distributions of the electrons emitted in the higher  $n$  continua of the  $1snl$   $\text{Li}^+$  ion are provided and compared with previous measurements and calculations.

## II. EXPERIMENT

The experiment was carried out at the atomic and molecular undulator beamline 10.0.1 of the Advanced Light Source Synchrotron Radiation Facility at Lawrence Berkeley National Laboratory. VUV radiation from a 4.5 m long 10 cm period undulator was monochromatized by a spherical grating monochromator. The electron spectra were measured using an end station designed for gas-phase angle-resolved studies and based on the Scienta SES-200 hemispherical analyzer [25]. The analyzer is rotatable in a plane perpendicular to the propagation direction of the beam of linearly polarized photons (the degree of linear polarization is estimated to be higher than 99%), allowing accurate electron angular distribution studies. The analyzer was operated at the constant pass energy of 40 eV with an electron energy resolution of 35 meV. The photon energy was calibrated using the photoelectron lines resulting from photoionization of xenon in the  $4d$ -subshells and the Auger electron lines resulting from the Auger relaxation of the  $4d_{5/2}$  hole in the  $\text{Xe}^+$  ion into the final state  $5s^25p^4\ ^1S_0$  of  $\text{Xe}^{2+}$ . The xenon gas was introduced into the interaction region by a separate gas inlet. A resistively heated metal vapor oven was used to generate an effusive beam of Li. The nozzle of a stainless steel crucible contained eight channels ( $d=0.8$  mm, 5 mm long) in a line, aligned parallel to the photon beam. This configuration increased the length of the interaction area without excessive broadening of the atomic beam. The operating temperature of the oven was in the range of 475–525 °C, at which the Li vapor pressure inside the crucible was  $\sim 3$  torr [26]. According to thermodynamical tables [26], less than 0.8% of the metal-vapor beam is molecular  $\text{Li}_2$  at 500 °C. Inelastic scattering peaks were observed at 1.89 eV lower kinetic energy from the  $1s2s$  ( $^1S$ ) and  $1s3s$  ( $^3S$ ) peaks. These peaks are due to electron-atom collisions, in which the Li atoms are excited to the  $1s^22p^1$  state and the electrons lose 1.89 eV of energy. In our spectra, the intensities of the inelastic scattering peaks are typically less than 0.4% of the measured electron lines. The presence of the inelastic scattering process indicates that the atom density of Li in the interaction region is in the order of  $10^{12}$  atoms/cm<sup>3</sup>. The final photoelectron spectra are sums of a number of spectra collected for a short time and aligned to the  $1s2s$  ( $^3S$ ) line ( $E_b=64.413$  eV), [27] in order to compensate for the energy shifts, caused by changing potentials of various surfaces near the interaction area as they become coated with lithium.

## III. THEORY

Two-electron photoionization processes, including satellites produced by inner-shell photoionization, are strictly for-

bidden in the one electron model of the atom and are a manifestation of electron correlations [28]. The growing use of synchrotron radiation has provided a large amount of data showing evidence of such phenomena that could not be explained in the one-electron model, but required the introduction of electron correlations into the theoretical model. Photoionization of an atom from the ground state into the continuum leaves the core-ionized residual ion in its lower energy state, corresponding to the so-called main line in a photoelectron spectrum (the electronic configurations of the initial atomic state and of the final ionic state are the same, except for the ejected electron) or in a state of higher energy, corresponding to the correlation satellite lines, in which a second electron has changed its principal (and/or its orbital quantum number) [28,29]. The nature of the mechanisms which are responsible for the existence of these correlation satellites is quite different depending upon whether the orbital quantum number 1 of the “second” electron has changed.

$$\Delta l = 0$$

The satellites corresponding to excited states of the ion in which the excited electron does not change its angular momentum during and after photoionization, have been well explained for many years by the shake theory [30,31]. The shake theory considers the excitation (or the ionization in case of double ionization) of the second electron as resulting from monopole relaxation of the system during and after ionization, without any exchange of angular momentum. When the photoelectron leaves the atom fast enough, the satellite transition intensity is approximately constant when the photon energy varies, and is equal to a constant fraction of the main line intensity. However, for low photoelectron kinetic energies, the remaining electrons have enough time to adjust adiabatically to the gradually changing screening potential of the nuclear charge. Consequently, the readjustment is the most effective for low photoelectron kinetic energies, giving rise to decreasing satellite intensity towards the ionization threshold. Shake-up satellites have been studied in the rare gases [32–34] and are now well understood [35].

Photoionization of  $1s$  electrons in Li, giving rise to the ( $1sns\ ^1,3S$ ) shake-up satellite states, can be written as:

$$1s^22s(^2S) + h\nu \rightarrow 1sns(^1,3S) + \epsilon p, \quad \text{with } n > 2, \quad (1)$$

with an intensity proportional to the following matrix element:

$$\langle \epsilon p | D | 1s \rangle \langle ns | 2s \rangle. \quad (2)$$

The first term describes single photoionization (the corresponding electron line is called the main line) and the second term accounts for the satellite excitation. The branching ratio between the satellite and main line is thus equal to  $|\langle ns | 2s \rangle|^2 / |\langle 2s | 2s \rangle|^2$ .

$$\Delta l \neq 0$$

The second category of satellites results from transitions in which the excited electron changes its orbital quantum

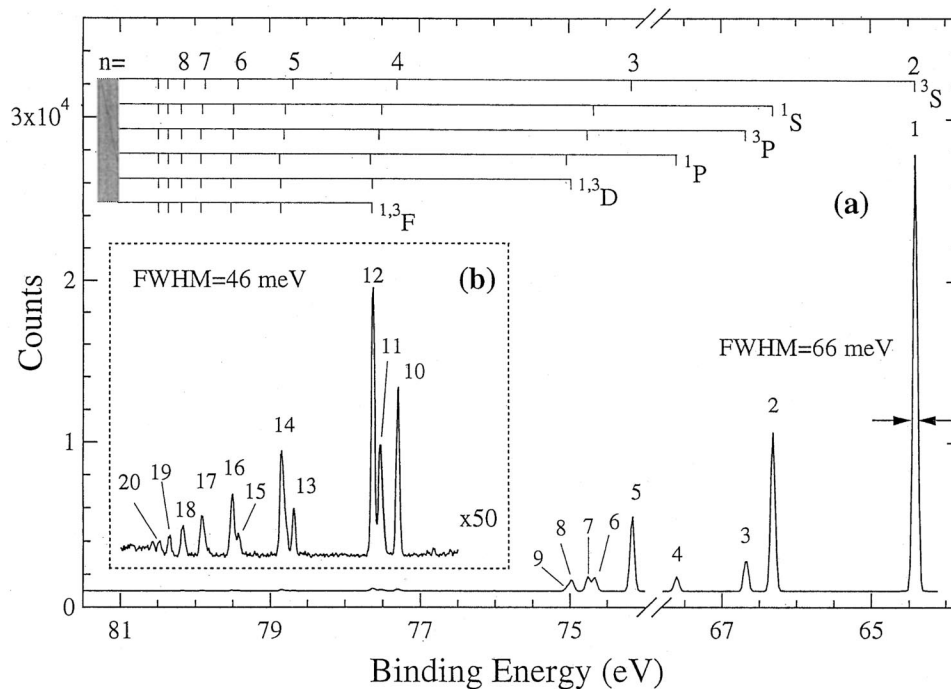


FIG. 1. Photoelectron spectrum of the  $\text{Li}^+$   $1snl$  satellites taken at 100 eV photon energy. Spectrum (a) covers the binding-energy range starting from the  $1s2l$  lines, and spectrum (b) shows the  $1snl$ ,  $n \geq 4$  lines at higher resolution. Peak assignments are given in Table I. The energy levels marked above the spectra are from Ref. [10].

number which implies an exchange of angular momentum between the residual ionic core and the outgoing photoelectron. These satellites have been observed in the early experimental photoionization studies in the rare gases [32–34] and were described as resulting from the virtual excitation of one of the remaining electrons in the atom resulting from its collision with the ejected photoelectron on its way out of the atom [36–40]. Satellites showing a change of two units in the orbital quantum number of the excited electron were thought to exist, but their intensity was believed at that time to be very low.

This virtual collisional process has received a number of different names, such as inelastic scattering [36], internal electron scattering [37,41], continuum-continuum configuration interaction [42], direct knock-out [43], or interchannel coupling [44]. In the past, the corresponding satellites have been also termed, improperly, conjugate shake-up satellites [11,34,45] to keep an analogy with the shake-up satellites when calculating the intensity of the satellites. However, this term is misleading since it could induce the wrong idea that it is a real mechanism, describing a different kind of photoionization process, while it just refers to the way some overlap integrals are calculated in the Hartree-Fock approximation [11,13]. Thus, we will not use this term in the following and will refer to this category of satellites as interchannel coupling (IC) satellites. All theories predict increasing intensity towards threshold for IC satellites. It should be noted, however, that shake-up satellite states can also be populated in this way. Consequently, it is difficult to identify the mechanisms producing the satellite lines based solely on the photon-energy dependency of these cross-sections near the ionization threshold. However, the variation of the intensities

of the satellite lines, as a function of photon energy, is still valuable information to assign the origin of various correlation satellites.

To go beyond the frozen-core Hartree-Fock approximation, various theoretical approaches have been used in order to introduce electron correlations. Among many others, the configuration interaction (CI) model [42,46] including the multiconfigurational HF (Ref. [47]) approach (MCHF), the many-body perturbation theory [48], and the  $R$ -matrix theory [49] have been the most productive, so far, in calculating two-electron photoionization cross sections.

Two-electron photoionization processes in the outer shell of the rare gases have been shown to result mainly from ground-state correlations (GSC), core relaxation (CR), and continuum state configuration interaction (CSCI). Such a classification however, should be considered with caution as it has been shown that it is gauge dependent [50]. Also, it may depend on the basis set of wave functions used to represent the initial and final states. In the alkali-atoms, the most intense two-electron processes involve electrons belonging to different shells, allowing to test specific classes of correlation effects. For the sodium atom, photoionization to states with  $\Delta l=0$  and 1, and double photoionization have been studied extensively, both experimentally [51–55] and theoretically [54,55], showing that core relaxation and continuum-continuum coupling are the dominant correlation effects, while ground-state correlations are almost negligible [51]. Strong photon energy dependences have also been measured for the  $\Delta l=1$  satellites following photoionization in the  $2p$  and  $2s$  inner-subshells [52,53].

For lithium atoms in the ground state, the transitions giving rise to the  $(1snl \ ^{1,3}L, l \geq 1)$  IC satellite states in photo-

TABLE I. Assignment of the  $1snl$  satellites lines in the Li  $1s$  photoelectron spectra of Figs. 1 and 2.

	Label	Assignment
$n=2$	1	$1s2s\ ^3S$
	2	$1s2s\ ^1S$
	3	$1s2p\ ^3P$
	4	$1s2p\ ^1P$
$n=3$	5	$1s3s\ ^3S$
	6	$1s3s\ ^1S$
	7	$1s3p\ ^3P$
	8	$1s3d\ ^{1,3}D$
	9	$1s3p\ ^1P$
$n=4$	10	$1s4s\ ^3S$
	11	$1s4s\ ^1S, ^3P$
	12	$1s4d\ ^{1,3}(L>1)$
$n=5$	13	$1s5s\ ^3S$
	14	$1s5s\ ^1S, ^{1,3}(L>0)$
$n=6$	15	$1s6s\ ^3S$
	16	$1s6s\ ^1S, ^{1,3}(L>0)$
$n=7$	17	$1s7l$ all terms
$n=8$	18	$1s8l$ all terms
$n=9$	19	$1s9l$ all terms
$n=10$	20	$1s10l$ all terms

ionization of the  $1s$  electrons can be written as

$$1s^2 2s(^2S) + h\nu \rightarrow 1snl(^{1,3}L) + \varepsilon l' \text{ or } \varepsilon l'', \quad (3)$$

with  $n > 2$  and  $l' = l - 1$  and  $l'' = l + 1$ .

In this work, we have used the  $R$ -matrix approximation to calculate the intensity of some of the measured satellites. Details about the method and its use to calculate photoionization cross sections in lithium have already been previously described [20,21,56,57]. In short, we have used the 29 states code, first developed to investigate the so-called hollow states of lithium, in order to calculate the term-resolved photoionization cross sections into the  $1snl\ ^{1,3}L$  ionic states  $\text{Li}^+$ , for  $n=2$  to 4 and  $l=1, 2$ , and 3. The CI expansion includes 151 basic configurations, giving 369 configuration couplings to construct the 29 target states. The radial wavefunctions for these orbitals in these configurations were evaluated using the CIV3 code. We have also calculated the angular distribution parameters for the electrons leaving the final ionic state in the  $1s2l$ ,  $1s3l$ , and  $1s4l\ ^{1,3}L$  states; with  $l=1$  and 2.

## IV. EXPERIMENTAL RESULTS

### A. Li $1s$ satellite spectra

Figure 1(a) shows the  $\text{Li}^+$   $1snl$  photoelectron spectrum covering the binding energy range from the  $1s2l$  diagram lines up to and across the double ionization threshold, measured at 100 eV photon energy at the ‘‘magic’’ angle of  $54.7^\circ$  relative to the polarization axis of the incoming pho-

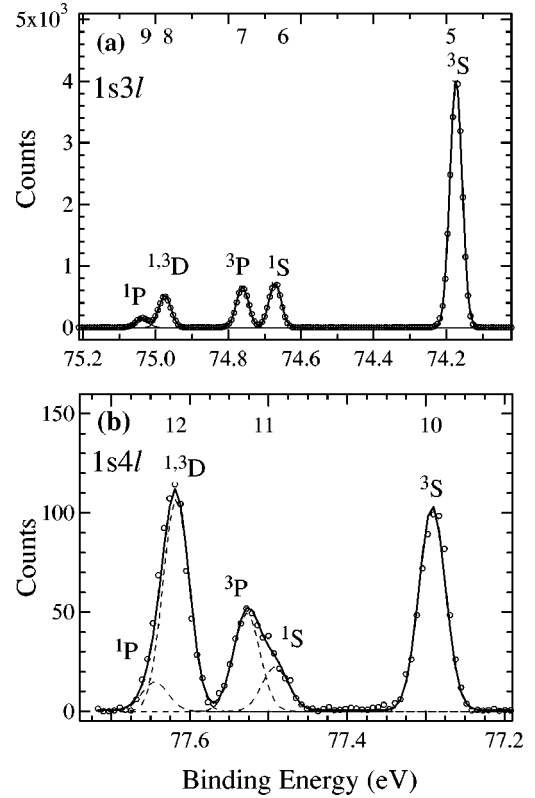


FIG. 2. The  $1s3l$  (a) and  $1s4l$  (b) terms in the Li  $1s$  photoelectron spectra measured at 110 eV photon energy. Numbering of the peaks is in accordance with Fig. 1 and Table I. A least-squares curve fit to the spectrum is shown by solid and dashed lines.

tons. In addition, the region of  $n \geq 4$  satellite transitions, shown in Fig. 1(b), was measured using higher experimental resolution.

The energy levels of the  $\text{Li}^+$   $1snl$  configurations, marked by vertical bars above the spectra, are from Baskin *et al.* [27]. The individual lines in the two spectra of Fig. 1 were fitted with Gaussian profiles. The linewidth of 66 meV (FWHM) was obtained for the  $\text{Li}^+$   $1s2l$  and  $1s3l$  lines in the spectrum (a), and 46 meV for the high-resolution spectrum (b). In spectrum (b), the Rydberg series of the  $1snl$  satellites is clearly resolved up to  $n=10$ . The individual satellite lines are numbered and their assignment is given in Table I, based on the comparison of the fitted peak positions with the energy levels from Baskin *et al.* [27].

All four terms ( $1s2s\ ^{1,3}S, 1s2p\ ^{1,3}P$ ) of the  $\text{Li}^+$   $1s2l$  final ionic state are completely resolved in Fig. 1(a). In the early measurements of the Li photoelectron spectra [5–9], only the main  $^3S$  line of the  $1s2l$  group was clearly separated whereas in more recent studies [14,15,58], all four terms are resolved, sometimes not completely for the  $^3P$  and  $^1S$  peaks.

Figure 2 concentrates on the region of the  $1s3l$  and  $1s4l$  satellite transitions of the Li  $1s$  photoelectron spectrum, which were measured at the highest energy resolution, allowing us to resolve the term structure of these transitions. The spectra in Fig. 2 were measured at 110 eV photon energy at the ‘‘magic’’ ( $54.7^\circ$ ) angle. The solid line through the data

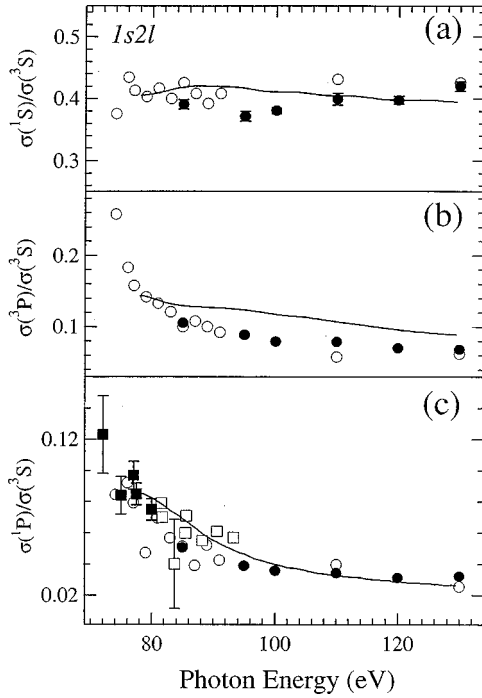


FIG. 3. Branching ratios of the terms within the  $\text{Li}^+ 1s2l$  group. Solid circles: this experiment, open circles: Ref. [8], and lines: our  $R$ -matrix calculations. Open squares in panel (c): Ref. [6], solid squares: Ref. [7].

points represents a least-squares fit of Gaussian profiles. The 20 meV spectrometer function and about 30 meV photon bandwidth, used for this measurement, account fully for the 37 meV linewidth determined from the fitting procedure. No additional Lorentzian broadening due to the natural width of the final ionic states was observed. In the case of isotropic thermal velocity distribution of the target atoms, an additional 60 meV Doppler broadening would contribute to the measured linewidth. Our much smaller linewidth of 37 meV indicates that the nozzle design of the oven gives a strong directionality to the emerging beams of the Li atoms, perpendicular to the axis of the electron detection, and therefore strongly suppresses the Doppler broadening in the electron energy distribution.

The  $1s3l$  group in Fig. 2(a) is resolved for all LS terms except the  $1^3D$  lines, which are separated only by 3 meV [25]. In the earlier Li  $1s$  photoelectron spectra [5–10] the term structure of the  $1s3l$  group was completely unresolved, and was partly resolved only in the most recent studies by Diehl *et al.* [58].

Figure 2(b) displays the  $1s4l$  satellite group consisting of the  $1s4s(1^3S)$ ,  $1s4p(1^3P)$ ,  $1s4d(1^3D)$  and  $1s4f(1^3F)$  lines, which are resolved except for the higher angular momentum terms  $1^3D$  and  $1^3F$ . The relative energy positions of the peaks were taken from Ref. [27] and were kept fixed during the fitting procedure. With fixed peak positions, the intensity of the unresolved peaks are represented more reliably. The binding energy region of the  $1s4l$  satellite lines show a recognizable unresolved structure only in the most recent studies [15,58].

TABLE II. Comparison of experimental and theoretical branching ratios of the  $1sns(1S)$  to the  $1sns(3S)$  lines for different  $n$ -values.

	$h\nu$ (eV)	$1sns\ 1S/3S$		
		$n=2$	$n=3$	$n=4$
This work				
Exp.	100	0.380(5)	0.178(4)	0.189(14)
Theory		0.414		
Exp.	130	0.420(8)	0.189(9)	0.180(12)
Theory	130	0.390		
<i>Other theoretical values</i>				
Larkins <i>et al.</i> , HF (Ref. [11])	151	0.361		
Armen <i>et al.</i> CI (Ref. [13])	100	0.394	0.082	
VoKy <i>et al.</i> , $R$ -matrix (Ref. [20])	100	0.46		
Yan (Ref. [22])		0.386	0.189	0.210
van der Hart and Greene (Ref. [23])		0.386	0.188	
Cooper (Ref. [24])		0.408	0.154	

## B. Branching ratios

### 1. The $1s2l$ group

The four LS-terms in the  $1s2l$  group are well resolved in energy and therefore a number of experimental and theoretical studies about their cross-sections and branching ratios are available. The branching ratios of the  $\text{Li}^+ 1s2l$  lines as a function of photon energy are shown in Fig. 3, where the

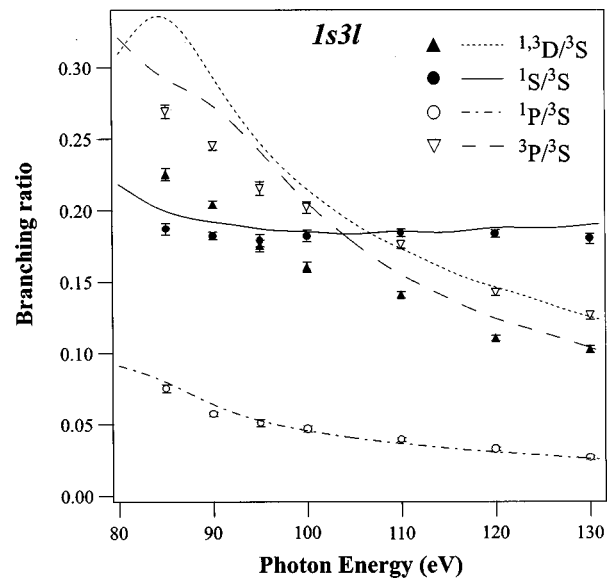


FIG. 4. Branching ratios of the  $\text{Li}^+ 1s3l$  lines to the  $1s3s(3S)$  line. Markers represent experimental data points and  $R$ -matrix calculations are shown by lines.

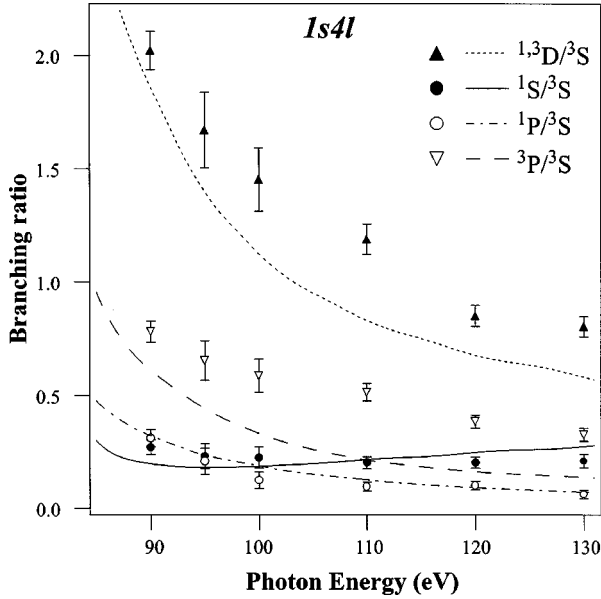


FIG. 5. Branching ratios of the  $\text{Li}^+$   $1s4l$  lines to the  $1s4s(^3S)$  line. Markers represent experimental data points and  $R$ -matrix calculations are shown by lines.

present data is compared with our  $R$ -matrix calculations and with most of the previous experimental results [6–8]. The ratios of the  $^1S$ ,  $^3P$ , and  $^1P$  lines to the  $1s2s(^3S)$  main line are given in panels (a), (b) and (c), respectively.

There is a good general agreement between the present and previous experiments. The  $^1S$  to  $^3S$  ratio given by Langer *et al.* [8] is slightly higher than our results (see Table II for a comparison of different experimental and theoretical results for the  $^1S$  to  $^3S$  ratio). This particular discrepancy might be due to inelastic scattering (discussed in Sec. II) of the electrons corresponding to the  $1s2s(^3S)$  peak, in which the electrons lose 1.89 eV of kinetic energy. The resulting secondary peak coincides with the  $^1S$  peak and can, if the atomic density of the target is high, contribute significantly to its intensity. In our measurement, the contribution from inelastic scattering process was found to be 1%. The  $^1P$  to

TABLE III. Comparison of experimental and theoretical branching ratios of the  $1s3l$  satellite lines.

	$h\nu$ (eV)	$^1S/^3S$	$^3P/^3S$	$^1P/^3S$	$^{1,3}D/^3S$
<i>This work</i>					
exp.	100	0.182(4)	0.202(4)	0.047(2)	0.160(3)
theory		0.185	0.206	0.045	0.215
exp.	130	0.180(5)	0.126(5)	0.027(2)	0.103(4)
theory		0.190	0.104	0.026	0.125
<i>Theory, other=</i>					
Larkins <i>et al.</i>	151	0.067	0.036	0.072	
HF (Ref. [11])					
Larkins <i>et al.</i>		0.193	0.045	0.016	
CI (Ref. [11])					
Armen <i>et al.</i>	100	0.062	0.000062	0.072	
(Ref. [13])					

$^3S$  ratio in panel (c) of Fig. 3 is compared also with the results of Gerard [6] and Ferrett *et al.* [7] which are not included in panels (a) and (b) since the  $^1S$  and  $^3P$  lines were not resolved in these studies). Good agreement between the experiments can be observed in this case.

## 2. The $1snl, n \geq 3$ groups

No previous experimental data is available on the individual branching ratios of the higher  $n$  satellite lines. The branching ratios from the present experiment over the photon energy range of 85–130 eV are shown in Fig. 4 for the  $1s3l$  group and in Fig. 5 for the  $1s4l$  group. Table III summarizes our experimental and calculated values and indicates also the earlier theoretical values. The  $^1S$  and  $^{1,3}P$  lines overlap strongly with the higher  $L$  lines in the satellite groups with  $n \geq 5$ . However, in order to be able to determine the branching ratios of the lines with different angular momentum, the intensity ratios of the lines with the same  $L$  were kept fixed:  $^1S$  to 20% of the intensity of the  $^3S$  line and  $^1P$  to 25% of the  $^3P$  line. These ratios were taken from the fit of the  $1s4l$  group, where they were found to be independent of photon energy and equal (within error bars) to the corresponding ratios in the  $1s3l$  group, thus providing a justification for extrapolation to the  $1s5l$  group.

The ratio of  $^1S$  to  $^3S$  in the  $1s3l$  and  $1s4l$  groups is, like for the  $1s2s$  lines, nearly constant over the displayed photon energy range (see also Table II). In contrast, the intensity of the higher angular momentum (IC) lines relative to the  $^3S$  line decreases rapidly towards higher photon energy. The high-angular-momentum ( $L \geq 2$ ) lines become the dominant terms in the spectra as  $n$  increases—the  $^{1,3}(D, F)$  lines are the strongest in the  $1s4l$  group at  $h\nu < 130$  eV. This trend seems to continue for  $n = 5$ , where the ( $^{1,3}L \geq 2$ ) to  $^3S$  ratio equals 2.7 at 90 and 1.2 at 130 eV photon energy, respectively. Similarly, the  $P$ -lines become stronger relative to the  $S$ -lines as  $n$  increases.

## C. Anisotropy parameter

The angle-dependent intensity of the emitted electrons is described by the differential cross section  $d\sigma/d\Omega$ . For completely linearly polarized light it is given by [59]:

$$d\sigma/d\Omega(\theta) = \sigma/4\pi [1 + \beta P_2(\cos(\theta))], \quad (4)$$

where  $\beta$  is the angular distribution parameter,  $\sigma$  the partial cross section and  $P_2(x) = (3x^2 - 1)/2$  the second-order Legendre polynomial.  $\theta$  is the angle between the electric field vector of the radiation (which lies in the horizontal plane in our case) and the direction of the outgoing electrons in a plane perpendicular to the light propagation vector.

The spectra shown in Fig. 1 for  $\theta = 54.7^\circ$  were also measured at  $\theta = 0^\circ$  and  $80^\circ$ . The theoretically predicted  $\beta$ -value of 2.00 for the  $^3S$  lines in the  $1s2l$  and  $1s3l$  groups was used to normalize the spectral intensities at different angles, and Eq. (4) was then used to extract the anisotropy parameters of other lines. We also calculated the  $1s2l$  anisotropy parameters using the method of branching ratios [60], where the intensity ratios of a pair of lines at three different angles are used. The advantage of this method is that it does not

TABLE IV. The anisotropy parameter  $\beta$  of  $L^+ 1snl$  satellite lines at 110 eV photon energy. Labels refer to Fig. 1.

Label	Assignment	Ref. 7	Ref. 8	Exp.	Calc.
1	$1s2s\ ^3S$	1.93(17)		2.00 <sup>a</sup>	2.00
2	$1s2s\ ^1S$	1.93(32)		1.98(4)	2.00
3	$1s2p\ ^3P$	1.30(20)	1.75	1.77(5)	1.77
4	$1s2p\ ^1P$	1.70(20)	1.65	1.71(5)	1.67
5	$1s3s\ ^3S$			2.00 <sup>a</sup>	2.00
6	$1s3s\ ^1S$			2.00(4)	2.00
7	$1s3p\ ^3P$			1.95(4)	1.98
8	$1s3d\ ^{1,3}D$			1.67(5)	1.60
9	$1s3p\ ^1P$			1.89(5)	1.97
10	$1s4s\ ^3S$			1.99(5)	
11	$1s4l\ ^1S, ^3P$			1.93(8)	
12	$1s4l\ ^1P, ^{1,3}(L>1)$			1.46(7)	
13	$1s5s\ ^3S$			1.94(8)	
14	$1s5l\ ^1S, ^3P$			2.07(16)	
	$1s5l\ ^1P, ^{1,3}(L>1)$			1.33(21)	
15	$1s6s\ ^3S$			1.98(12)	
16	$1s6l\ ^1S, ^{1,3}(L>0)$			1.56(20)	

<sup>a</sup>Theoretical value, fixed.

require explicit normalization of the spectra measured at different angles nor does it rely on a known  $\beta$ -value of one line in the spectrum. However, the error bars can become quite large if the lines have similar  $\beta$ -values. Also, the  $\beta$ -value of the  $1s2s(^3S)$  was found equal to two within the error bars using this method.

The anisotropy parameters from the present experiment and  $R$ -matrix calculations are given in Table IV. The experimental error bars represent the statistical uncertainties of the line intensities and include also a  $\pm 1^\circ$  error in the angle of the electron detection. The experimental  $\beta$ -values for the  $1sns(^{1,3}S)$ ,  $n=2-6$  lines are, within error bars, equal to 2.0 as predicted by theory. The  $\beta$ -values for the  $P$ -lines are significantly lower than 2.0 for the  $1s2l$  group, but the difference is smaller for the  $1s3l$  lines. The  $\beta$ -values for the  $^{1,3}D$  line in the  $1s3l$  group are lower than the one for the  $S$ - and  $P$ -lines, although they show also an anisotropic angular distribution. The  $\beta$ -values of high-angular-momentum lines can be followed from  $n=3$  to 5. For  $n=4$  and 5, there is some admixture of the  $^1P$  terms, but the effect is expected to be weak, since the cross sections for photoionization to the  $1snp\ ^1P$  states are quite small. The anisotropy of the high  $L$  lines is reduced, which is an indication that there is a significant population of the highest  $L$  final states as they become available ( $^{1,3}F$  for  $n=4$  and  $^{1,3}G$  for  $n=5$ ).

## V. DISCUSSION

### A. Comparison of theory and experiment

Agreement between the branching ratios from the present  $R$ -matrix theory and experiment is good for the  $^1S$  and  $^1P$  lines in the  $1s2l$  group, although the calculated  $^1S$  to  $^3S$  ratio decreases slightly with photon energy, whereas a small increase is observed experimentally. A significant discrep-

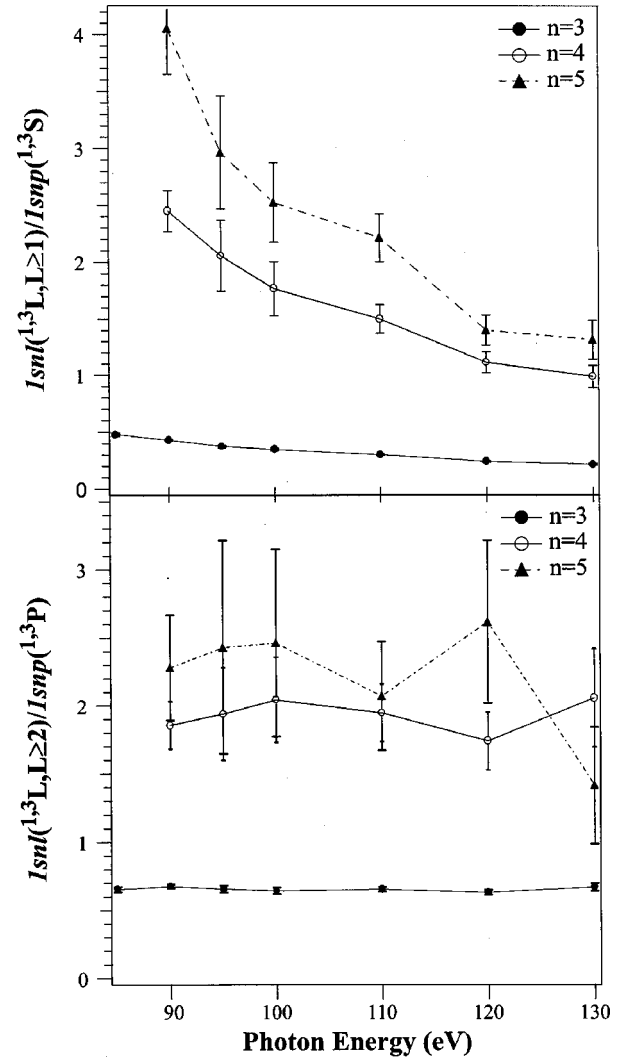


FIG. 6. Experimental ratios of the lines with  $L \geq 1$  to the shake-up lines in different  $1snl$  satellite groups (upper panel) and the ratios of the high-angular-momentum lines with  $L \geq 2$  to the  $P$ -lines (lower panel).

ancy is observed for the  $^3P$  line, where the calculations overestimate the cross section to the  $1s3p\ ^3P$  final ionic state. There is a much stronger disagreement of the present experimental results, as has been noted by previous works [6–8], with earlier theoretical photoionization cross sections by Armen *et al.* [13], which were based on the calculation of overlap integrals for the IC  $^{1,3}P$  satellites. These results represent correctly the ratio of the main lines ( $^1S$  to  $^3S$ ), but predict negligible intensity for the  $^3P$  CC line and about two times larger cross-section for the  $^1P$  line than observed.

The  $1sns(^{1,3}S)$  shake-up lines for  $n \geq 3$  have a significant intensity. In addition, the transitions to the final states of higher angular momenta ( $^{1,3}P, ^{1,3}D$ ) have a considerable intensity in the  $1s3l$  satellite spectrum [see also Fig. 2(a)] and especially in the  $1s4l$  spectrum [Fig. 2(b)], where the  $^{1,3}(D,F)$  and  $^3S$  peaks have nearly equal intensities. The results of our  $R$ -matrix calculations, also shown in Figs. 3 and 4, are in excellent agreement with the experimental data for the  $^1S$  and  $^1P$  satellite states, and are still in reasonable agreement for the  $^{1,3}P$  and  $^{1,3}D$  (including also  $^{1,3}F$  for  $n$

=4) satellite states. The numerical comparison of the branching ratios measured in this work with the results of various theoretical calculations, as given in Table III for the  $1s3l$  group, illustrates the good agreement between our experimental and theoretical  $R$ -matrix results. This confirms that the  $R$ -matrix approach is also well suited for calculating the transitions to ( $l \geq 1$ ) angular momentum states, as already suggested by the earlier comparisons for the  $1s2l$  group of lines [18].

### B. Comparison of branching ratios in different $1snl$ satellite groups

The character of the satellite lines with high angular momenta ( $L \geq 2$ ) can be determined individually from our high-resolution measurements of the  $1snl$   $n=3$  and 4 groups. Branching ratios of the lines with  $L > 2$  ( $D, F, \dots$ ) to the  $P$ -lines for different  $n$  are shown in the lower panel of Fig. 6. For  $n=3$  and 4, sum of the  $^1P$  and  $^3P$  line intensities, as obtained by least-squares curve fitting, was used. For  $n=5$ , the  $^1P$  peak overlaps strongly with the much stronger  $^{1,3}(D, F, \dots)$  peak and its intensity cannot be determined directly. It is clear from Fig. 6 that the ( $D, F, \dots$ ) to  $P$  ratio is photon energy independent over the given range for  $n=3$  and 4. For  $n=5$ , no significant trends can be observed. For higher  $n$ -values the statistical uncertainty becomes too large for drawing conclusions. The average measured values for the  $^{1,3}(L > 1)$  to  $^{1,3}P$  ratio are 0.655(15), 1.93(12), 2.2 (4), and 3.1 (1.3) for  $n=3, 4, 5$ , and 6, respectively.

In contrast to this behavior, the ratios of the  $L \geq 1$  to the  $S$ -lines, shown in the upper panel of Fig. 6 for up to  $n=5$ , are strongly photon energy dependent. Combining the results shown in Figs. 6 leads to the conclusion that the satellite lines with  $L \geq 1$  show the same energy dependence, that is clearly different from the behavior of the  $S$ -lines. Therefore, while the lines with  $L=0$  are a clear manifestation of shake-up processes, the lines with  $L \geq 1$  are produced mainly by interchannel coupling. It should be noted also that the relative intensities of the shake-up satellites, in comparison with the intensities of the CC satellites, decreases dramatically with increasing values of the principal quantum number  $n$ .

### C. Anisotropy parameters

The anisotropy parameters can provide additional information necessary to differentiate between mechanisms of satellite creation. The  $\beta$ -parameters of the  $1sns$  ( $^{1,3}S$ ) lines do not show a significant deviation from the value of two, which corresponds to the angular distribution of a single outgoing  $p$  continuum wave. This value is also predicted by the shake-up model, where the  $1s$  electron leaves the atom as a  $p$ -wave. Although previous measurements of the angular

asymmetry parameter  $\beta$  for several of the satellite lines in helium have strongly suggested a significant intensity of the high ( $nd$   $\text{He}^+$ ) states [61–63], we provide here, to the best of our knowledge, the first direct measurements of the angular behavior of well resolved  $nd$  satellites ( $1s3d$  and  $1s4d$   $\text{Li}^+$  states). For all ( $l \geq 1$ ) satellites, the values of the asymmetry parameter deviate from two. This further supports the conclusion based on the branching ratios, that all satellites with a nonzero angular momentum, are created mainly by interchannel coupling.

## VI. CONCLUSION

In the work presented here, term-resolved branching ratios of the electron correlation satellite lines in lithium were determined for the transitions to the  $1snl$ ,  $n=2, 3$ , and 4 singly-ionized states over a broad photon energy range below the double-ionization threshold. We were able to completely resolve, to the best of our knowledge, for the first time, some of the highly-excited satellites such as the  $^{1,3}D$  states, bringing experimental evidence that the transitions to these states have considerable intensity. In addition, relative intensities of the well-resolved  $^3S$  lines were determined up to  $n=6$ .

In the case of  $1s2l$  lines, our branching ratios agree reasonably well with previous results. The branching ratios for the higher  $n$  satellite lines, not reported previously, show strong enhancement of the transitions involving a change of the angular momentum of the excited electron over the shake-up process, especially at lower photon energies. Transitions to the higher angular momentum states  $^{1,3}D$  were found to be strong within the  $1s3l$  group and especially within the  $1s4l$  group, where the  $1s4d(^{1,3}D)$  line is the strongest. The appearance and strength of these lines is a direct measure of configuration interaction in the continuum. The photon energy dependency of the intensity of all ( $l \geq 1$ ) momentum lines is the same and does not depend on the values of one.

The anisotropy parameters were determined for the  $1snl$ ,  $n=2, 3$ , and 4 lines. The  $\beta$ -parameters of  $^{1,3}P$  lines, arising from the continuum-continuum state coupling, increase significantly from the  $1s2l$  to  $1s3l$  group. Photoionization to the higher angular momentum states is more isotropic, especially in the  $1s4l$  group.

## ACKNOWLEDGMENTS

This work was supported by the U.S. Department of Energy, Office of Science, Basic Energy Sciences, Chemical Sciences Division. The Advanced Light Source is supported by the Materials Science Division of the U.S. Department of Energy. The authors would like to thank S. T. Manson, C. H. Greene, and E. J. McGuire for stimulating discussions.

- 
- [1] R. P. Madden and K. Codling, Phys. Rev. Lett. **10**, 516 (1963).  
 [2] U. Fano and J. W. Cooper, Rev. Mod. Phys. **40**, 441 (1968).  
 [3] K. Schulz, G. Kaindl, M. Domke, J. D. Bozek, P. A. Heimann,

- A. S. Schlachter, and J. M. Rost, Phys. Rev. Lett. **77**, 3086 (1996).  
 [4] A. Menzel, S. P. Frigo, S. B. Whitfield, C. D. Caldwell, and M.

- O. Krause, Phys. Rev. A **54**, 2080 (1996), and references therein.
- [5] S. Krummacher, V. Schmidt, J.-M. Bizau, D. L. Ederer, P. Dhez, and F. J. Wuilleumier, J. Phys. B **15**, 4264 (1982).
- [6] P. Gérard, Thesis, University Paris-Sud (1985).
- [7] T. A. Ferrett, D. W. Lindle, P. A. Heimann, W. D. Brewer, U. Becker, H. G. Kerkhoff, and D. A. Shirley, Phys. Rev. A **36**, 3172 (1987).
- [8] B. Langer, J. Viehhaus, O. Hemmers, A. Menzel, R. Wehlitz, and U. Becker, Phys. Rev. A **43**, 1652 (1991).
- [9] F. J. Wuilleumier, in *Review of Fundamental Processes and Applications of Atoms and Ions*, edited by C. D. Lin (World Scientific, Singapore, 1993), pp. 283–356.
- [10] L. Journal, Thesis, University Paris-Sud, 1995; see also Ref. [17] where his experimental results are compared with the results of *R*-matrix calculations.
- [11] F. P. Larkins, P. D. Andeney, and K. G. Dylla, J. Electron Spectrosc. Relat. Phenom. **22**, 141 (1981).
- [12] A. Lisini, P. G. Burke, and A. Hibbert, J. Phys. B **23**, 3767 (1990).
- [13] G. B. Armen, B. I. Craig, F. P. Larkins, and J. A. Richards, J. Electron Spectrosc. Relat. Phenom. **51**, 183 (1990).
- [14] S. Diehl, Ph.D Thesis, Université Paris-Sud, Orsay, 1998.
- [15] F. J. Wuilleumier, S. Diehl, D. Cubaynes, J.-M. Bizau, and E. T. Kennedy, J. Electron Spectrosc. Relat. Phenom. **88**, 41 (1998).
- [16] D. Cubaynes, S. Diehl, L. Journal, B. Rouvellou, J.-M. Bizau, S. Al Moussalami, F. J. Wuilleumier, N. Berrah, L. VoKy, P. Faucher, A. Hibbert, C. Blancard, E. T. Kennedy, T. J. Morgan, J. Bozek, and A. S. Schlachter, Phys. Rev. Lett. **77**, 2194 (1996).
- [17] H. L. Zhou, S. T. Manson, L. VoKy, P. Faucher, F. Bely-Dubau, A. Hibbert, S. Diehl, D. Cubaynes, J.-M. Bizau, L. Journal, and F. J. Wuilleumier, Phys. Rev. A **59**, 462 (1999).
- [18] Y. Azuma, F. Koike, J. W. Cooper, T. Nagata, G. Kuluk, E. Shigemasa, R. Wehlitz, and I. A. Sellin, Phys. Rev. Lett. **79**, 2419 (1997).
- [19] M. T. Huang, R. Wehlitz, Y. Azuma, L. Pibida, I. A. Sellin, J. W. Cooper, M. Koike, H. Ishijima, and T. Nagata, Phys. Rev. A **59**, 3397 (1999).
- [20] L. VoKy, P. Faucher, A. Hibbert, J. M. Li, Y. Z. Qu, J. Yan, J. C. Chang, and F. Bely-Dubau, Phys. Rev. A **57**, 1045 (1998).
- [21] L. VoKy, P. Faucher, H. L. Zhou, A. Hibbert, Y. Z. Qu, J. M. Li, and F. Bely-Dubau, Phys. Rev. A **58**, 3688 (1998).
- [22] Z. C. Yan, Phys. Rev. A **60**, R3358 (1999).
- [23] H. W. van der Hart and C. H. Greene, Phys. Rev. Lett. **81**, 4333 (1998).
- [24] J. W. Cooper, Phys. Rev. A **59**, 4825 (1999).
- [25] N. Berrah, B. Langer, A. A. Wills, E. Kukk, J. D. Bozek, A. Farhat, and T. W. Gorczyca, J. Electron Spectrosc. Relat. Phenom. **101-103**, 1 (1999).
- [26] A. N. Nesmeyanov, *Vapor Pressure of the Chemical Elements* (Elsevier, Amsterdam, 1963).
- [27] S. Baskin and J. O. Stoner, *Atomic Energy Levels and Grottrian Diagrams*, Vol. 1 (North-Holland, Amsterdam, 1975).
- [28] T. Aberg, in *Photoionization and Other Probes of Many-Electron Interactions*, edited by F. J. Wuilleumier (Plenum Press, New York, 1976), p. 49.
- [29] M. O. Krause, in *Photoionization and Other Probes of Many-Electron Interactions*, edited by F. J. Wuilleumier (Plenum Press, New York, 1976), p. 133.
- [30] A. Middal, J. Phys. (USSR) **4**, 449 (1941).
- [31] T. A. Carlson, C. W. Nestor, Jr., T. C. Tucker, and F. B. Malik, Phys. Rev. **169**, 27 (1968).
- [32] J. A. R. Samson, Phys. Rev. Lett. **65**, 2861 (1969).
- [33] M. O. Krause and F. J. Wuilleumier, J. Phys. B **5**, L143 (1972).
- [34] F. J. Wuilleumier and M. O. Krause, Phys. Rev. A **10**, 242 (1974).
- [35] V. Schmidt, Rep. Prog. Phys. **55**, 1483 (1992).
- [36] T. N. Chang, T. Ishihara, and R. T. Poe, Phys. Rev. Lett. **27**, 838 (1971).
- [37] T. N. Chang and R. T. Poe, Phys. Rev. A **12**, 1432 (1975).
- [38] S. L. Carter and H. P. Kelly, J. Phys. B **9**, 1887 (1976).
- [39] S. L. Carter and H. P. Kelly, Phys. Rev. A **16**, 1525 (1977).
- [40] S. L. Carter and H. P. Kelly, Phys. Rev. A **24**, 170 (1981).
- [41] T. A. Carlson and C. W. Nestor, Phys. Rev. A **8**, 2887 (1973).
- [42] R. L. Martin and D. A. Shirley, Phys. Rev. A **13**, 1475 (1976).
- [43] M. Ya Amusia, in *Vacuum Ultraviolet Radiation Physics*, VUV 10 Proceedings, edited by F. J. Wuilleumier, Y. Petroff, and I. Nenner (World Scientific, Singapore, 1993), p. 3.
- [44] S. T. Manson, J. Electron Spectrosc. Relat. Phenom. **9**, 21 (1976).
- [45] U. Gelius, J. Electron Spectrosc. Relat. Phenom. **5**, 985 (1974).
- [46] U. Becker and D. A. Shirley, Phys. Scr. **T31**, 56 (1990).
- [47] C. E. Froese-Fischer, Comput. Phys. Commun. **9**, 31 (1975).
- [48] H. P. Kelly, Adv. Theor. Phys. **2**, 75 (1968).
- [49] P. G. Burke and K. T. Taylor, J. Phys. B **8**, 2620 (1975).
- [50] A. Dalgarno and H. Sadeghpour, Phys. Rev. A **46**, R3591 (1992).
- [51] F. J. Wuilleumier, L. Journal, B. Rouvellou, D. Cubaynes, J. M. Bizau, Z. Liu, J. Liu, M. Richter, P. Sladeczek, K.-H. Selbman, and P. Zimmermann, Phys. Rev. Lett. **73**, 3074 (1994).
- [52] M. Richter, J.-M. Bizau, D. Cubaynes, T. Menzel, F. J. Wuilleumier, and B. Carré, Europhys. Lett. **12**, 35 (1990).
- [53] D. Cubaynes, J.-M. Bizau, M. Richter, and F. J. Wuilleumier, Europhys. Lett. **14**, 747 (1991).
- [54] D. Cubaynes, L. VoKy, F. J. Wuilleumier, B. Rouvellou, A. Hibbert, P. Faucher, J.-M. Bizau, L. Journal, H. E. Saraph, and J. Bely-Dubau, Phys. Rev. A **57**, 4432 (1998).
- [55] J. C. Liu and Z. W. Liu, J. Phys. C **27**, 4531 (1994).
- [56] L. Journal, D. Cubaynes, J.-M. Bizau, S. Al Moussalami, B. Rouvellou, F. J. Wuilleumier, L. VoKy, P. Faucher, and A. Hibbert, Phys. Rev. Lett. **76**, 30 (1996).
- [57] S. Diehl, D. Cubaynes, J.-M. Bizau, L. Journal, B. Rouvellou, S. Al Moussalami, F. J. Wuilleumier, E. T. Kennedy, N. Berrah, C. Blancard, T. J. Morgan, J. Bozek, A. S. Schlachter, L. VoKy, P. Faucher, and A. Hibbert, Phys. Rev. Lett. **76**, 3915 (1996).
- [58] S. Diehl, 1988 (private communication).
- [59] J. Cooper and K. N. Zare, J. Chem. Phys. **48**, 942 (1968).
- [60] A. Kivimäki, E. Kukk, J. Karvonen, J. Mursu, E. Nommiste, H. Aksela, and S. Aksela, Phys. Rev. A **57**, 2724 (1998).
- [61] J.-M. Bizau, F. J. Wuilleumier, P. Dhez, D. L. Ederer, T. N. Chang, S. Krummacher, and V. Schmidt, Phys. Rev. Lett. **48**, 588 (1982).
- [62] D. W. Lindle, P. A. Heimann, T. A. Ferrett, and D. A. Shirley, Phys. Rev. A **31**, 714 (1985).
- [63] R. Wehlitz, B. Langer, N. Berrah, S. B. Whitfield, J. Viehhaus, and U. Becker, J. Phys. B **26**, L783 (1993).